SLAC-PUB-2988
October 1982
(T/E)

PHOTON-PHOTON COLLISIONS*

David L. Burke
Stanford Linear Accelerator Center
Stanford University, Stanford, California 94305

Sommaire — Des études des collisions photon-photon sont revues avec une attention particulière donnée aux resultats nouveaux presentés à cette conférence. Ceux-ci incluent des résultats sur la spectrosopie des mésons légers et sur la diffusion inélastique profonde électron-photon. Un travail considérable a été jusqu'à maintenant accompli sur la production de résonances dans les collisions $\gamma\gamma$.

Des études préliminaires, de grandes statistiques, de la fonction de structure du photon $F_2^\gamma(x,Q^2)$ sont présentées et des commentaires sont faits sur les problèmes qu'il reste à résoudre.

Abstract — Studies of photon-photon collisions are reviewed with particular emphasis on new results reported to this conference. These include results on light meson spectroscopy and deep inelastic $e\gamma$ scattering. Considerable work has now been accumulated on resonance production by $\gamma\gamma$ collisions. Preliminary high statistics studies of the photon structure function $F_2^\gamma(x,Q^2)$ are given and comments are made on the problems that remain to be solved.

1. General Remarks — The advent of high-energy high-luminosity e^+e^- storage rings has led to productive studies of photon-photon collisions. As shown[1] by C. F. Weizsacker and E. J. Williams, the electromagnetic field produced by a charge moving with relativistic velocity is equivalent to a flux of virtual photons with a characteristic spectrum,

$$dN_\gamma/dk \propto 1/k \quad , \tag{1}$$

and with an angular divergence that is quite small for large energies,

$$\theta_\gamma \sim m/E \quad . \tag{2}$$

It is clear that colliding electron beams, such as those at PEP and PETRA, have associated with them well-collimated colliding beams of nearly-real photons. As illustrated in Fig. 1, various final states can be produced by these photon-photon collisions; for two real (massless) photons, the state X is restricted to have even charge conjugation and, by Yang's theorem, the spin cannot be J = 1. The latter condition is relaxed if one of the beam electrons is scattered at a finite angle so that the q^2 of the corresponding photon is not zero.

Detailed analyses of the kinematics of the process shown in Fig. 1 can be found in the literature,[2] but we note here that invariant masses produced by photon-photon collisions range continuously from threshold values up to the maximum allowed by the beam energy E_b. The differential cross section in $s_x = m_x^2$ is determined predominantly by the bremstrahlung spectrum noted in (1). Roughly,

$$\frac{d\sigma(ee \to eeX)}{ds_x} \propto \left(\ln \frac{E_b}{m_e}\right)^2 \cdot \ln \frac{E_b}{m_x} \cdot \frac{\sigma_{\gamma\gamma \to x}(s_x)}{s_x} \tag{3}$$

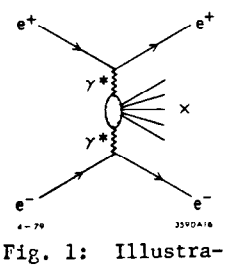

Fig. 1: Illustration of the process ee → eeX.

By contrast, the annihilation channel is characterized by events that occur at one invariant mass $s = 4E_b^2$ (ignoring radiative

*Work supported by the Department of Energy, contract DE-AC03-76SF00515.

(Raporteur talk presented at the XXI International Conference on High Energy Physics, Paris, France, July 26-31, 1982.)

corrections), and the cross section falls like $1/E_b^2$. The logarithms in formula (3) arise from integrations over the phase space allowed the motion of the $\gamma\gamma$ center of mass. Note that $2 \cdot \ln(2 \cdot E_b/m_X)$ is just the length of the rapidity interval available for a state with mass m_X. The cross section for the production of X by two real photons is $\sigma_{\gamma\gamma \to X}(s_X)$. More generally, if $\sigma(s_X, q_1^2, q_2^2)$ depends upon the masses of the incident photons, then relation (3) must be rewritten in terms of a sum over photon helicities and helicity dependent cross sections. As noted above, however, unless one of the scattered beam electrons is detected at a finite angle, most of the observed events correspond to $q_1^2 \simeq q_2^2 \simeq 0$, and replacing $\sigma(s_X, q_1^2, q_2^2) \to \sigma(s_X, 0, 0)$ is not too bad of an approximation.[2,3]

The problem for the experimentalist is to detect the final state X (notice that the $\gamma\gamma$ CMS is not at rest in the lab), and to separate the two-photon produced states from backgrounds due to the annihilation channel. This latter problem is solved in two distinct ways. Exclusive measurements, in which all final state particles are detected, can be isolated from the annihilation channel by making use of the kinematics of the two-photon process. Events are selected that display masses $m_X << 2E_b$ and low net transverse momenta relative to the beam $|p_t| \simeq 0$ (typically $|p_t| < 100$ MeV/c). This latter property is due to the small divergence of the equivalent photon beams (Eq. (2)). Two-photon events can also be "tagged" by detecting one of the outgoing beam electrons at small angles with respect to the beam line. Both of these techniques have been successfully used to study two-photon collisions.

The list of topics for which data have been reported in the literature covers most aspects of strong interaction physics. It includes:

- QED: $(\gamma\gamma \to l\bar{l})$
- spectroscopy: $(\gamma\gamma \to |q\bar{q}\rangle)$
- hadronic pair production: $(\gamma\gamma \to m\bar{m})$
- total hadronic cross sections:
- high-p_t phenomena:
  - single particle inclusive distributions ($\gamma\gamma \to \pi$,K,etc. + anything)
  - jet structures ($\gamma\gamma \to q\bar{q}$)
- deep inelastic $e\gamma$ scattering: $(e\gamma \to e$ + hadrons)
  - photon structure functions

I have chosen to present in this talk results from only two of these areas — spectroscopy (Section 2) and deep inelastic $e\gamma$ scattering — (Section 3). These are extremely interesting subjects and are areas in which the study of photon-photon collisions can play an important role in our understanding of the strong interaction. The most glaring omission in this talk will be the absence of any discussion of the studies of high-p_t phenomena. No new results on this topic were reported at this conference, and the interested reader is referred to the review given at the Bonn Conference last year.[4]

2. Spectroscopy

A. Introduction — The production of a quark-antiquark meson resonance R (spin $J \neq 1$ and $C = +$) by two real photons is described by the diagram shown in Fig. 2a. The production cross section is related to the partial width of the decay process $R \to \gamma\gamma$,

$$\sigma_{\gamma\gamma \to R}(s) \propto (2J+1) \cdot \Gamma_{R \to \gamma\gamma} \cdot BW(s) \qquad (4)$$

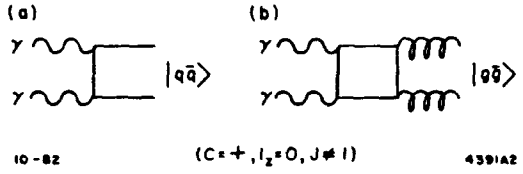

Fig. 2: Two-photon production of (a) quark-antiquark bound states and (b) glue-glue bound states. The quantum numbers of a state that couples to two real photons are shown in the figure.

where BW(s) is an appropriate Breit-Wigner line shape, and the spin factor is needed since the partial width is defined in terms of an average over the various possible initial spin states in the decay process. Hence a measurement of the production rate for $ee \to eeR$ is also, by (3) and (4), a measure of the partial width of R into two photons (if the spin of R is known).

Knowledge of $\Gamma_{R \to \gamma\gamma}$ is of interest because it is a probe of the $|q\bar{q}\rangle$ bound-state wave function,

$$\Gamma_{|q\bar{q}\rangle \to \gamma\gamma} \propto \frac{e_q^4}{(2J+1)} \cdot \sum_{j=-J}^{J} \int |\langle \gamma\gamma | M | q\bar{q}, j \rangle|^2 \, d^3k \quad . \tag{5}$$

The quark charge is e_q (in units of e) and the matrix element is written for unit charges. The wave functions of bound states of light quarks are highly relativistic, and the problem is usually approached within the theoretical framework of SU(3). The assumption of nonet symmetry implies that the overlap integral is the same for all members of a given multiplet, so the ratios of various partial widths are given by the quark charges and mixing angles derived from mass formulae. The partial widths of heavy quark resonances (e.g., the $\eta_c(2980)$), should be computable with the non-relativistic potential models that are used to describe the appropriate -onium spectrum. Unfortunately, no data exist yet on the two-photon production of any of these heavier states.

One of the more interesting problems in the study of the light meson spectrum is to arrive at an understanding of the role played by the purely gluonic bound states $|gg\rangle$ expected to exist due to the non-Abelean nature of QCD. As noted above, the coupling of a resonance to two photons is determined to first order by the charge of the constituents that make up the state in question. The coupling of a gluonic bound state to $\gamma\gamma$ proceeds only through the OZI-suppressed box diagram shown in Fig. 2b. Somewhat more generally[5] if $|R\rangle$ is a linear combination of $|q\bar{q}\rangle$ and $|gg\rangle$,

$$|R\rangle = \cos\theta \; |q\bar{q}\rangle + \sin\theta \; |gg\rangle \tag{6}$$

then we would expect $\Gamma_{R \to \gamma\gamma} \propto |\cos\theta|^2$. By comparison, the production of $|R\rangle$ in a "glueball favored" channel, such as the prompt photon decay $J/\psi \to \gamma R$ shown in Fig. 3,

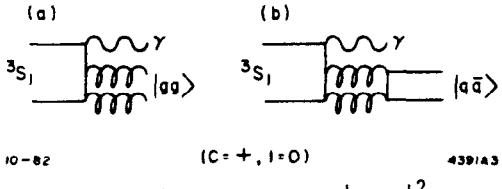

Fig. 3: Prompt-photon decays of an ortho-quarkonium bound state, for example, $J/\psi \to \gamma +$ (a) glue-glue and (b) quark-antiquark.

would proceed with rates $\propto |\sin\theta|^2$. Naively then, states that are easily produced by photon-photon collisions would seem to not be good candidates for states that are predominantly $|gg\rangle$.

Four quark resonances $|q\bar{q}q\bar{q}\rangle$ are expected to be rather loosely bound and quite broad. These states literally "fall apart" into pairs of vector particles,

$$|q\bar{q}q\bar{q}\rangle \to |q\bar{q}\rangle_v + |q\bar{q}\rangle_v \quad . \tag{7}$$

If this is the case, then the vector-meson-dominance model of the photon leads one quite naturally to look for four-quark states in $\gamma\gamma$ collisions.[6]

B. Pseudoscalar Mesons — Measurements of the $\gamma\gamma$ partial width of a number of known resonances have now been reported in the literature, and in fact, are beginning to appear as standard entries in the Particle Data Group tables.[7] The first resonance to be detected[8] in photon-photon collisions at e^+e^- machines was the $\eta'(958)$. Along with results for the π^0 and $\eta(550)$ partial widths obtained from Primakoff production experiments, this provided the complete set of values for the 0^{-+} pseudoscalar multiplet given in Table I. The beautiful agreement between the measured widths and those

expected from SU(3) is probably the strongest evidence to date that quarks carry fractional charge.[9]

C. Tensor Mesons and the θ(1650) — Measurements of partial widths for the 2^{++} tensor mesons f(1270) and A_2(1310) have been on the market for some time now, but reported[10] at this conference is a first measurement for the f'(1515). This measurement has been made by studying the $K\bar{K}$ final state. Limits are also set on the coupling of the θ(1650) to γγ. This latter resonance has been observed[11] in the prompt-photon decay $J/\psi \to \gamma\theta$, with the subsequent decay of the θ into both ηη and $K\bar{K}$. The production and decay angular distributions observed in the prompt photon studies somewhat favor a $J^{PC} = 2^{++}$ assignment, and so discussion of this state is included in this section.

Table I. Radiative Widths of the Pseudoscalar Mesons

	$\Gamma_{\gamma\gamma}$ (keV)			
	Data		Theory[c]	
			Fractional Quark Charges	Integral Quark Charges
π^0	7.95	× 10^{-3}[a]	input	input
η	0.324 ± 0.046[a]		0.390	0.720
η'	5.8 ± 1.1[b]		6.1	26
	5.0 ± 0.5[b]			
	5.4 ± 1.0[b]			

[a]Ref. 7 [b]Ref. 8 [c]Ref. 9

Shown in Fig. 4 are the spectra obtained by TASSO[10] for the two-photon production of K^+K^- and $K^0_S\bar{K}^0_S$. The K^+K^- events are selected to have net $p_t < 100$ MeV/c and the kaons have been identified by the time-of-flight technique. There is a clear peak at the position of the f'(1515) with few events seen at the θ(1650). Some care should be taken here since the efficiency of the time-of-flight identification of the kaons falls at the higher masses and is essentially zero at $m_{KK} = 1.9$ GeV/c^2. The $K^0_S\bar{K}^0_S$ spectrum seen in Fig. 4b (obtained from events with four charged prongs with net $p_t < 150$ MeV/c) also exhibits a peak at the mass of the f'(1515). The partial widths obtained from these two spectra agree with each other within statistical uncertainty, and the TASSO group reports,

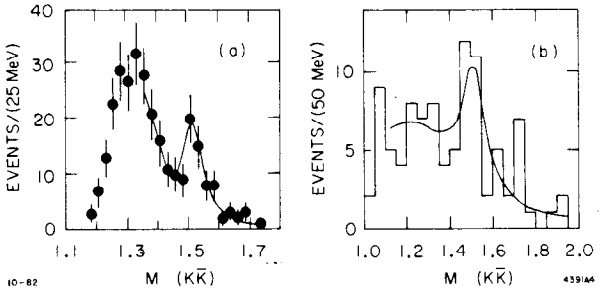

Fig. 4: (a) The K^+K^- spectrum produced by γγ collisions, and (b) the corresponding spectrum for $K^0_S\bar{K}^0_S$.

$$\Gamma_{f' \to \gamma\gamma} \cdot BR_{f' \to K\bar{K}} = 0.15 \pm 0.03 \,^{+0.03}_{-0.04} \text{ keV} \quad , \tag{8}$$

and

$$\Gamma_{\theta \to \gamma\gamma} \cdot BR_{\theta \to K\bar{K}} < 0.5 \text{ keV} \quad (95\% \text{ C.L.}) \quad , \tag{9}$$

where the branching ratios include both kaon charge states. The Mark II group has made a similar study with about one-third of the luminosity of the TASSO experiment and gives only the limits,

$$\Gamma_{f' \to \gamma\gamma} \cdot BR_{f' \to K\bar{K}} < 0.25 \text{ keV} \quad (95\% \text{ C.L.}) \quad , \tag{10}$$

and,

$$\Gamma_{\theta \to \gamma\gamma} \cdot BR_{\theta \to K\bar{K}} < 0.4 \text{ keV} \quad (95\% \text{ C.L.}) \quad . \tag{11}$$

The values given in (8) through (11) assume that the spin of the θ is J = 2 and that the f' and the θ are produced with helicity λ = 2 by real photons. The results are sensitive to the helicity structure of the production reaction because the acceptance

of the detectors depend upon the angular distribution of the produced kaon pairs. If the f' is assumed to be created entirely with $\lambda = 0$, then the partial width obtained by TASSO from the K^+K^- channel would[10] be 0.5 ± 0.1 keV.

A summary of the reported[7,10,12,13] measurements of the partial widths of the 2^{++} tensor mesons is given in Fig. 5; new results reported at this conference are underlined in the figure. The error bars are the reported statistical contributions only, so the scatter in the data are an indication of the level of agreement between the various experiments. Note also that all points, except the Crystal Ball (CB) measurement of the f(1270), assume that the production process for J = 2 proceeds through helicity $\lambda = 2$. The Crystal Ball was able to study the helicity structure of the process $\gamma\gamma \to f \to \pi^0\pi^0$ and found the data consistent with $\lambda = 2$, although the best fit included a contribution from $\lambda = 0$ of ≃10%. This multiplet is believed to be ideally mixed with the $f = (u\bar{u} + d\bar{d})/\sqrt{2}$ and the $A_2 = (u\bar{u} - d\bar{d})\sqrt{2}$, while the f' is the purely strange $|s\bar{s}\rangle$ state. These quark assignments predict that the $\gamma\gamma$ partial widths of these resonances should be in the ratio 25:9:2. With the average of the measured values of the f(1270) as input, this SU(3) prediction is shown in Fig. 5. Since the mass of the f'(1515) is larger than the other two states, a phase space correction (scaled like m^3) has been included in the figure. The agreement is not perfect, but given the uncertainty regarding the helicity structure of these reactions, it is actually remarkably good. It has been argued[14] that the $\gamma\gamma$ partial width of the f'(1515) is extremely sensitive to the fraction of non-$s\bar{s}$ quark pairs in its wavefunction. The value reported above places[10] an upper limit of 1% on the amount of non-$s\bar{s}$ quark admixtures in the f'(1515).

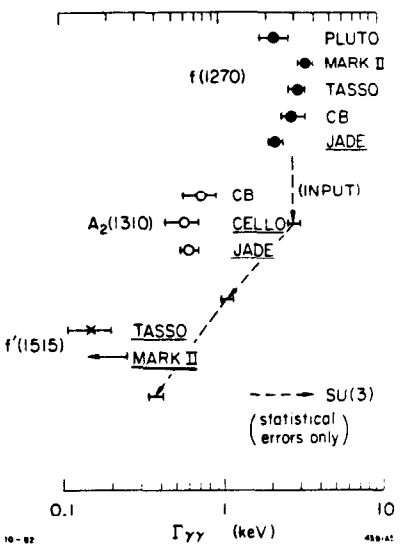

Fig. 5: Summary of measured partial widths of the 2^{++} tensor mesons. The underlined results were reported at this conference.

The limits (9) and (11) on the coupling of the θ(1650) to γγ are actually not yet very stringent. The branching fraction of the θ to $K\bar{K}$ is not known, but may be as small as 10-20%, while that of the f'(1515) is probably quite large. If the θ is predominantly a spin-2 $s\bar{s}$ state, then its coupling to γγ would presumably be comparable to that of the f'. The data cannot rule out a partial width $\Gamma(\theta \to \gamma\gamma)$ of the order 0.1-0.2 keV. If the θ is a 2^{++} glue-glue resonance, then a rough estimate of its width can be made by noting that the presence of two electromagnetic vertices in the quark loop in Fig. 2b means that the process is dominated by the u-quark. The rate for the decay $|gg;\ J = 2\rangle \to \gamma\gamma$ should be of the order of that for $f(1270) \to \gamma\gamma$ times an OZI suppression factor. This latter suppression can be estimated as the square root of the Zweig factor of the φ(1020), which is ≃100. Roughly then, $\Gamma(|gg;\ J = 2\rangle \to \gamma\gamma)$ may be of order a few tenths of a keV. This is certainly consistent with the data. Unfortunately, it also appears to be about the same size as that for the $s\bar{s}$ hypothesis.

D. The $\pi^+\pi^-\pi^+\pi^-$ Final State — The four pion final state produced by photon-photon collisions was one of the first to be studied.[15] It was found that the cross section exhibits a large enhancement near $m_{4\pi} \simeq 1.5$ GeV/c^2. The early data are shown in Fig. 6. This enhancement was found to be mostly due to $\rho^0\rho^0$ production, but the statistics of these data limited the sophistication of the analyses that could be done by the experimenters. The magnitude of the cross section, however, is extremely large for a single channel, and vector-meson-dominance cannot easily explain this effect.[15]

Preliminary, high-statistics data (70 pb^{-1}) have been reported at this conference by the TASSO group.[10] The observed spectrum of events, uncorrected for detection efficiency or photon flux, is shown in Fig. 7. High-lighted in this

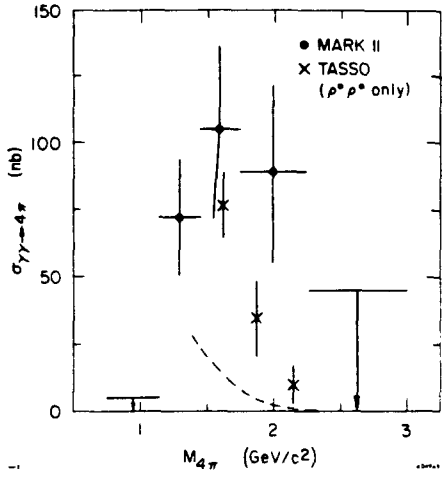

Fig. 6: The $\pi^+\pi^-\pi^+\pi^-$ cross section as first observed in $\gamma\gamma$ collisions.

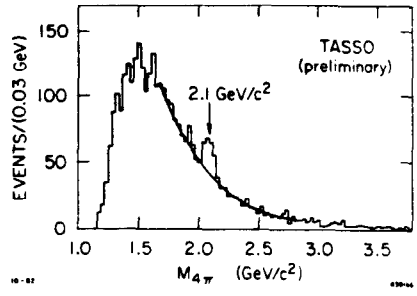

Fig. 7: High statistics $\pi^+\pi^-\pi^+\pi^-$ spectrum reported by TASSO. The curve is a polynomial fit to the region 1.6 GeV/c^2 to 3.0 GeV/c^2.

figure is the presence of a narrow peak with a mass of 2.10 ± 0.01 GeV/c^2, and a measured Gaussian width of 94 ± 21 MeV/c^2 FWHM. This latter value should be compared with the intrinsic resolution of the TASSO detector which is ≈60 MeV/c^2 FWHM. The statistical significance of the signal is derived by fitting the background with a polynomial as shown in the figure. Simply counting the number of events above this background in the mass range 2.0-2.2 GeV/c^2 yields 342-258 = 84 events, or a 5.2 standard deviation effect. This is a rather conservative technique since it ignores the tails of the Breit-Wigner which would contribute to a signal derived from a fit to the data. The TASSO group also estimates the partial width as

$$(2J+1) \cdot \Gamma_{\gamma\gamma} \cdot BR(\pi^+\pi^-\pi^+\pi^-) = 1.6 \pm 0.4 \text{ (statistical) keV} \quad . \qquad (12)$$

The spin factor (see Eq. (4) and discussion) has not been determined and the detection efficiency was computed by assuming that the four pions are produced according to phase space. The established resonance closest to this peak is the h(2040), a 4^{++} state with m = 2.040 ± 0.020 and total width = 150 ± 50 MeV/c^2 that has been observed[7] in high-statistics spectrometer experiments in the $\pi\pi$, KK, and perhaps $p\bar{p}$ channels. Although the mass of the h is reasonably close to that quoted above, the width of the peak in the $\gamma\gamma$ process may be considerably smaller than 150 MeV/c^2. No limits are given in the PDG table for a possible decay of the h(2040) into four pions. The most direct way to resolve this possibility will be to examine the $\gamma\gamma \to \pi\pi$ and KK channels in this mass range. The experimental resolution on the mass of the two-body final state will be considerably better, but this channel is complicated by the QED process $\gamma\gamma \to \mu^+\mu^-$ and $\gamma\gamma \to e^+e^-$ which are large and must be suppressed experimentally. No results have been reported yet.

The TASSO group has also done a more detailed analysis of the complete set of events in Fig. 7. They find that the spectrum below ≈2.0 GeV/c^2 is almost totally dominated by the $\rho^0\rho^0$ final state while above 2.0 GeV/c^2 the 4π final state is prevalent. Little $\rho^0\pi\pi$ is seen anywhere, and the peak at 2.1 GeV/c^2 does not appear to contain any ρ^0's whatsoever. A two-body partial wave analysis of the $\rho^0\rho^0$ spectrum below 2.0 GeV/c^2 rules out significant 0^- and 2^- contributions, while either an isotropic distribution or a combination of 0^+ and 2^+ give equivalently good fits to the data; the limited geometrical acceptance of the detector makes it difficult to separate these two possibilities. A particular limit has been set on the production and decay of the θ(1650),

$$\Gamma_{\theta\to\gamma\gamma} \cdot BR_{\theta\to\rho^0\rho^0} < 1.2 \text{ keV (95\% C.L.)} \quad . \qquad (13)$$

The θ apparently can account for no more than about one-third of the $\rho^0\rho^0$ events found in the region between 1.5 GeV/c^2 and 1.9 GeV/c^2. This may be of interest in light of a recently reported[16] observation of the decay $J/\psi \to \gamma\rho^0\rho^0$. The $\rho^0\rho^0$ spectrum seen in this decay is concentrated at masses below 2.0 GeV/c^2, but limited statistics prevent any detailed study of the $\rho^0\rho^0$ system. Work by the Mark III at SPEAR may ultimately provide a larger data sample.

3. Deep Inelastic eγ Scattering: The Photon Structure Function

A. Introduction — We turn now to a rather different view of photon-photon collisions. As mentioned in the opening remarks, if one of the scattered beam electrons is detected at finite angles as shown in Fig. 8, then the mass of the corresponding photon is not near zero, and some care must be taken in writing the production cross section. Particularly if $Q^2 = -q^2$ is large, then the process is more correctly thought of as deep inelastic eγ scattering, where the target is chosen from the flux of nearly-real photons associated with the undetected beam electron. In complete analogy with deep inelastic electron-nucleon scattering, the eγ process can be written in terms of particular combinations of longitudinal and transverse structure functions that describe the unknown hadronic vertex in Fig. 8. With the purely QED factors from the upper vertex explicitly included, we can write quite generally,[17]

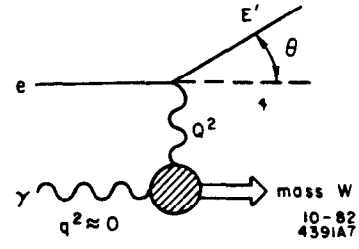

Fig. 8: Diagram for the deep inelastic scattering process eγ → e + hadrons.

$$\frac{d\sigma(e\gamma \to e + \text{hadrons})}{dxdy} = \frac{16\pi\alpha^2 E_b E_\gamma}{Q^4}\left[xy^2 \cdot F_1^\gamma(x,Q^2) + (1-y)\cdot F_2^\gamma(x,Q^2)\right] \qquad (14)$$

where x and y are the usual scaling variables,

$$x = \frac{Q^2}{2\nu} = \frac{Q^2}{Q^2 + W^2} \qquad (15)$$

and,

$$y = \frac{\nu}{2E_b E_\gamma} = 1 - \frac{E'}{E}\cdot\cos^2(\theta/2) \quad . \qquad (16)$$

Formula (14) must be convoluted with spectrum of target photons to describe the overall process ee → ee + hadrons. As in the case of electron-nucleon scattering, the variable y is approximately the fractional energy lost by the detected beam electron and, in the parton model, x is the momentum fraction of the target parton struck by the high Q^2 probe. In this case the target parton is quite literally a constituent of a real photon. Before discussing the physics in Eq. (14) we note that in experiments done to date the factor xy^2, which is proportional to $\sin^2(\theta/2)$, is small compared to $(1-y)$. At the level of statistics currently available, the observed cross section is sensitive only to F_2^γ. Experimenters have so far ignored the contribution of F_1^γ and have used measurements of the cross section to extract F_2^γ.

The function $F_2^\gamma(x,Q^2)$ has the well-known interpretation as the momentum and charge weighted distribution of hard constituents in the target photon. In the absence of gluon bremstrahlung, the simplest diagram is shown in Fig. 9 with,

$$F_2^\gamma(x,Q^2) \simeq x \cdot \sum_q e_q^2 \cdot \left[q(x,Q^2) + \bar{q}(x,Q^2)\right] \quad . \qquad (17)$$

The charge of the struck quark is e_q, and $q(x,Q^2)$, which describes the disassociation of the target photon into $q\bar{q}$, also contains a factor of e_q^2. To see the form that $q(x,Q^2)$ will take, first consider the purely QED process $e\gamma \to e + l\bar{l}$. This is described by Fig. 9 with the quark-antiquark pair replaced by a lepton pair. The

distribution of leptons in a photon, $l(x,Q^2)$, is just the familiar[18] double-peaked function that describes pair production,

$$l(x,Q^2) = \frac{\alpha}{2\pi} \cdot \left[x^2 + (1-x)^2\right] \cdot \ln \frac{W^2}{m_l^2} \quad . \qquad (18)$$

Shown in Fig. 10 are measurements made by PLUTO[19] and CELLO[12] of the leptonic structure function of the photon. The data agree well with the simple form implied by (17) and (18).

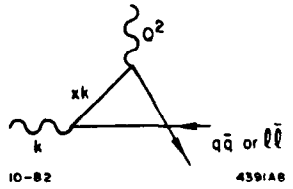

Fig. 9: Quark-parton model for the hadronic vertex shown in Fig. 8.

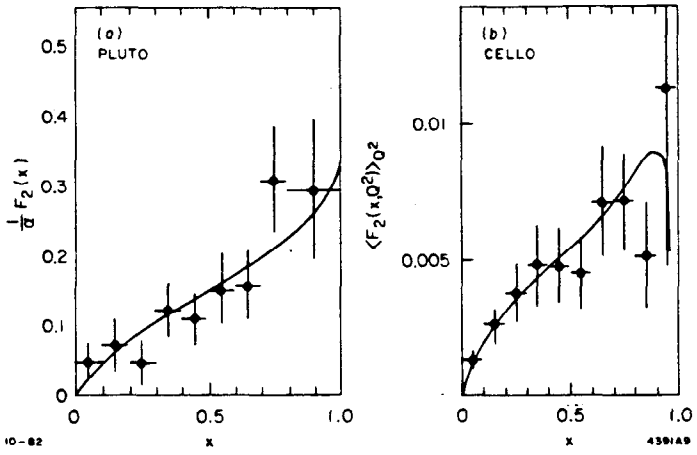

Fig. 10: Leptonic structure function of the photon. The curves are QED calculations.

B. Hadronic Structure of the Photon — It is clear that the quark-parton model prediction for the hadronic structure function F_2^γ is given by Eqs. (17) and (18) with the lepton mass replaced by the appropriate quark masses,

$$F_2^\gamma \simeq 3 \cdot \frac{\alpha}{\pi} \cdot \sum_q e_q^4 \cdot x \cdot \left[x^2 + (1-x)^2\right] \cdot \ln \frac{W^2}{m_q^2} \quad , \qquad (19)$$

where a color factor of 3 has been included. This corresponds to the simplest point-like behavior — the photon enters directly into the hard-scattering process as in Fig. 9. By contrast, if the photon behaves strictly as a hadron (VDM), then instead of rising at large x, we would expect F_2^γ to fall with increasing x as nuclear structure functions are known to do. One estimate[17] gives

$$F_2^\gamma \text{ (VDM)} \simeq 0.11 \cdot (1-x) \quad . \qquad (20)$$

Equations (19) and (20) are compared in Fig. 11, and are seen to be drastically different for $x \gtrsim 0.2$. The real interest in measurements of F_2 stems from the fact that, at large Q^2 and W and for $x \gtrsim 0.3$, the hadronic (e.g., VDM) contributions to F_2^γ are expected to be small, thus possibly allowing perturbative QCD calculations to successfully describe the deviations of F_2^γ from the simple Born parton model prediction. Leading-log calculations have been completed[20] and estimates of the next order contributions have also been made.[21] The leading-log calculation gives (for light quark contributions)

$$F_2^\gamma(x,Q^2) \propto h(x) \cdot \ln \frac{Q^2}{\Lambda^2} \qquad (21)$$

where Λ is the scale parameter of QCD. The function h(x) is quite similar to the parton model prediction, but differs at large x where gluon bremstrahlung softens the spectrum of quarks in the photon. The function (21) is shown in Fig. 11 for $Q^2 = 3$ GeV^2 and the relatively large value $\Lambda = 500$ MeV. For smaller values of the QCD prediction is closer to the parton model curve. Notice that F_2^γ in (21) exhibits an explicit scale breaking $\propto \ln Q^2$. For heavier quarks (e.g., charm) it is probably more correct to use the parton model form $\ln W^2/m_q^2$, but an exact treatment of the threshold has not been given.

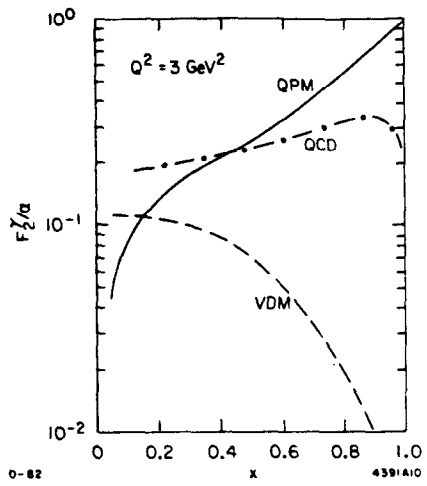

Fig. 11: Comparison of the hadronic structure function of the photon as expected from three different models of the photon. The QCD curve is the leading-log prediction for Λ = 500 MeV.

The earliest measurement of F_2^γ was made[22] by the PLUTO collaboration. The scattered beam electrons were detected in electromagnetic calorimeters arrayed along the beam line and covering the angular range between 100 mrad and 250 mrad. Only events with >0.75 GeV of energy visible in the remainder of the detector were used in the measurement. The published results, based on 2500 nb^{-1}, are shown in Fig. 12. What is shown is the value of $F_2^\gamma(x,Q^2)$ averaged over the range $1 < Q^2 < 15$ GeV; the average value $\langle Q^2 \rangle$ for these data is 5 GeV^2. The lowest order (L.O.) QCD prediction for this range of Q^2 is shown in the figure for Λ_{LO} = 200 MeV, and the higher order expectation is given for $\Lambda_{\overline{MS}} = 200$ MeV. Notice that these computations were done with different renormalization schemes, so the H.O. curve cannot be directly compared with the L.O. one. The QCD scale has essentially been adjusted in each case to fit the data. A major uncertainty in these data arises because the mass W must be reconstructed from the hadronic system that is seen in the central part of the detector. Since all detectors have limited geometrical acceptance, only a "visible" W is measured and it is necessary to unfold x_{true} from x_{vis} with a model for the production of the hadronic system. The PLUTO analysis was done by generating $q\bar{q}$ pairs (Fig. 9) and then decaying the hadronic system according to a phase-space model with limited-p_t about the $q\bar{q}$ direction in the $\gamma\gamma$ CMS. The final results are claimed to be insensitive to the details of this model. Despite this problem, these data are clearly inconsistent with the VDM prediction, and indicate that a real photon contains a considerable component of large x constituents.

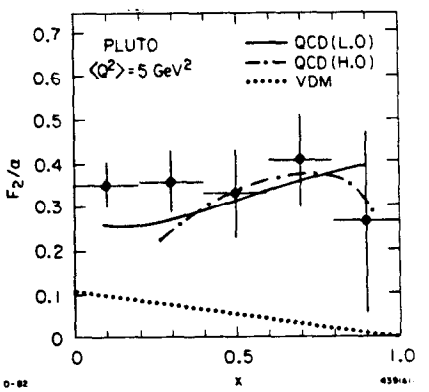

Fig. 12: $F_2^\gamma(x)$ averaged over $1 < Q^2 < 15$ GeV^2 measured by PLUTO. The curves labeled QCD also include the VDM contribution.

Preliminary, higher-statistics data were presented at this conference by the CELLO[12] and JADE[13] collaborations. These groups have not attempted to unfold the true x distribution from the observed events, but instead have compared various Monte Carlo calculations to the raw data. These are shown in Figs. 13 and 14. The CELLO data correspond to 11.2 pb^{-1} with an average $\langle Q^2 \rangle \simeq 8.4$ GeV^2, while the JADE results are from 20 pb^{-1} with $\langle Q^2 \rangle \simeq 23$ GeV^2. The Q^2 values differ because the two experiments had different acceptances for the scattered beam electrons. Both measurements were made by requiring $W_{vis} > 1$ GeV, and since $x_{vis} = Q^2/(Q^2 + W_{vis}^2)$ then the higher Q^2 data from JADE are peaked at higher x_{vis} than the CELLO data.

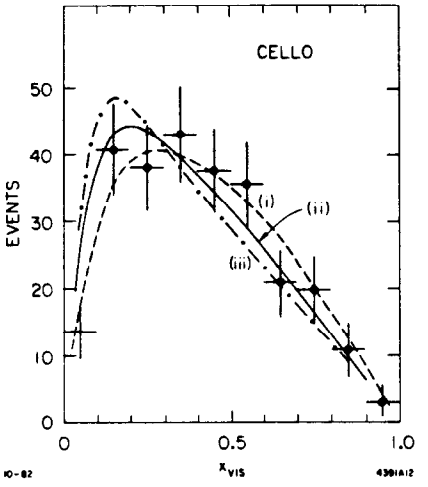

Fig. 13: Distribution in x_{vis} of events seen by the CELLO detector. The curves are predictions for (i) the QPM, (ii) a combination of QCD for (u,d,s) quarks and the QPM for the charm quark, and (iii) QCD for all quark species. The three cases are independently normalized to the data.

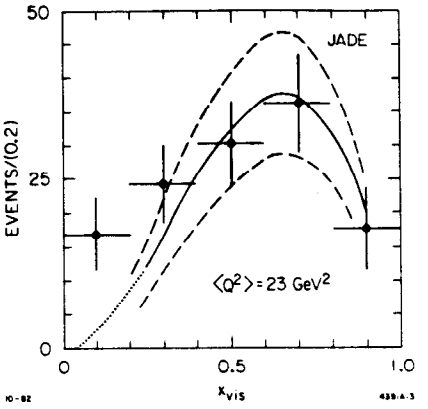

Fig. 14: Distribution in x_{vis} of events seen by the JADE detector. The solid curve is the prediction of a second order QCD calculation with $\Lambda_{\overline{ms}} = 200$ Mev. The upper dashed curve is the same calculation done with $\Lambda_{\overline{ms}} = 100$ Mev, and the lower curve corresponds to $\Lambda_{\overline{ms}} = 400$ Mev.

The CELLO data in Fig. 13 are compared with the shapes expected from the parton model (Eq. (19)), the lowest order QCD calculation (Eq. (21)), and a combination in which the contribution of the charm quark is taken from (19) and the light quarks are treated with (21). In all cases the curves are normalized to the data. The shapes of the distributions are not very different. The absolute normalization, however, of the QCD prediction is determined by the value of Λ and these data are consistent with values $0.1 < \Lambda_{LO} < 0.2$. The sensitivity of F_2^γ to the value of Λ is shown more directly in Fig. 14. Here the JADE data are compared for three different values of $\Lambda_{\overline{ms}}$ with a QCD calculation that includes terms $\propto \ln(\ln Q^2/\Lambda^2_{\overline{ms}})$. A fit to the data for $x_{vis} > 0.4$ gives,

$$\Lambda_{\overline{ms}} = 0.22 \begin{matrix} +0.10 \\ -0.07 \end{matrix} \text{ GeV} \quad . \tag{22}$$

It should be noted that in these calculations, the charm quark was treated as a light quark. If (19) is used instead of (21) for the charm quark, then the value of $\Lambda_{\overline{ms}}$ from the JADE data becomes[13] 0.18 — a change of about 20%.

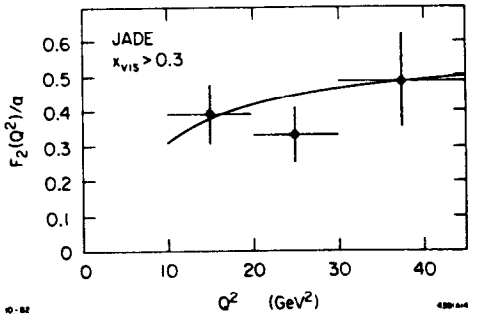

Fig. 15: The JADE data binned in Q^2. Only events with $x_{vis} > 0.3$ have been included in this plot. The curve is the ln Q^2 behavior expected from point-like constituents in the photon.

A second distinctive feature of both the parton model and QCD is that F_2^γ is expected to be proportional to $\ln Q^2$ (at fixed x), rather than vanish like a power of $1/(\ln Q^2)$ as do structure functions of nucleons. The JADE data, binned in Q^2 and averaged over the region $x_{vis} > 0.3$, are shown in Fig. 15 and are seen to be consistent with the expected point-like behavior. The PLUTO results were also examined[22] in this way and found to display this property.

C. Promise and Problems of Deep Inelastic eγ Scattering — The data above represent a relatively small amount of luminosity and it can be expected that, in the near future, data samples 4-10 times as large will be available. At that time measurements of the photon structure functions will no longer be statistics limited. In principle, this could become a very sensitive way of determining the QCD scale parameter Λ in whatever renormalization scheme is desired. There are, however, several serious theoretical and experimental problems, some of which have already been alluded to in the above discussion of data. Firstly, it hasn't been proven yet that the perturbative QCD series converges anywhere in x. It is known that for $x < 0.3$ the lowest order QCD prediction is unstable, thus indicating that non-perturbative contributions are important in that region. Also, values of x very near 1.0 correspond to the lowest W values and various threshold effects not described by perturbative diagrams become important.[23] Secondly, there is no proper treatment yet of the heavier quarks. As noted above, the value of $\Lambda_{\overline{MS}}$ derived from the JADE data changes by ≃20% when the contribution of the charm quark is evaluated with the parton model instead of QCD.

On the experimental side there should be some concern that events with invariant masses as low as 1 GeV/c^2 are included in the measurements of F_2^γ. Indeed, the measurements are dominated by invariant masses between 1 and 3 GeV/c^2. It could be expected that contributions from resonances and thresholds will be suppressed at large Q^2, but this is somewhat dangerous. It must be noted that some discrepancies exist between the observed invariant mass distributions and those predicted by the QCD Monte Carlos used by the experimenters. This is particularly true in the CELLO data[12] which is at a lower Q^2 than the JADE results. But certainly the most important task facing the experimentalists is to successfully unfold the true x distributions from the observed events. The problem is that events produced at low x, where perturbative QCD calculations are unreliable, are shifted to larger x_{vis} when part of the final state is missed by the detector ($x_{vis} = Q^2/(Q^2 + W^2_{vis})$). The unfold procedure will always have some inherent model dependence. This can be avoided by detecting both scattered beam electrons, but event yields are then reduced.

4. Conclusions — I would like to conclude by noting that photon-photon physics has become a standard feature of the elementary particle physics landscape. The topics included in this talk are quite divergent in character, yet center on our understanding of the strong interaction and hadronic structure. Study of the spectrum of resonant states produced by γγ collisions is by now an old game, but always with new and useful results. It also seems clear that, when viewed as a particle in its own right, the photon displays a structure that is remarkably point-like even at modest Q^2. We should expect, then, that PEP and PETRA will continue to be excellent places to study this physics.

REFERENCES

[1] WILLIAMS (E. J.) Proc. R. Soc. London, 1933, A139, 163.
WEIZSACKER (C. F.) Z. Phys., 1934, 88, 612.

[2] BRODSKY (S. J.), KINOSHITA (T.), TERAZAWA (H.), Phys. Rev. D, 1971, 4, 1532.
BONNEAU (G.), GOURDIN (M.), MARTIN (F.), Nucl. Phys. B, 1973, 54, 572.
FIELD (J. H.), Nucl. Phys. B, 1980, 168, 477.

[3] KESSLER (P.), contributed paper 0761 to this conference.

[4] WEDEMEYER (R. J.), Proceeding of the 1981 Symposium on Lepton and Photon Interactions at High Energies, ed. W. Pfeil.

[5] ROSNER (J. L.), Phys. Rev. D, 1981, 24, 1347.

[6] LI (B. A.), LIU (K. F.), SLAC-PUB-2783, 1981.
ACHASOV (N. N.), DEVYANIN (S. A.), SHESTAKOV (G. N.), Phys. Lett., 1982, 108B, 134.

[7] PARTICLE DATA GROUP, Phys. Lett., 1982, 111B.
[8] ABRAMS (G.S.) et al., Phys. Rev. Lett, 1979, 43, 477; JENNI (P.), Proceedings of International Workshop on $\gamma\gamma$ Collisions, Amiens, France, 1980, ed. G. Cochard and P. Kessler.
BARTEL (W.) et al., JADE Collaboration, Phys. Lett., 1982, 113B, 190.
BEHREND (H. J.) et al., CELLO Collaboration, DESY 82-008, and talk at this conference.
[9] CHANOWITZ (M. S.), Phys. Rev. Lett., 1980, 44, 59.
[10] LUKE (D.), TASSO Collaboration, presentation at this conference.
[11] EDWARDS (C.) et al., Phys. Rev. Lett., 1982, 48, 458.
FRANKLIN (M.E.B.) et al., Bull. Am. Phys. Soc., 1982, 27, 553.
See also BLOOM (E.), raporteur at this conference.
[12] BEHREND (H. J.), CELLO Collaboration, presentation at this conference, and contributed papers 0562, 0739, and 0740.
[13] HEINZELMANN (G.), JADE Collaboration, presentation at this conference
[14] ROSNER (J. L.), University of Minnesota preprint, July 1982.
[15] BRANDELIK (R.) et al., TASSO Collaboration, Phys. Lett., 1980, 97B, 448.
BURKE (D. L.) et al., Phys. Lett., 1981, 103B, 153.
[16] BURKE (D. L.) et al., Phys. Rev. Lett., 1982, 49, 632.
[17] For a good summary of the formalism of deep inelastic $e\gamma$ scattering see PETERSON (C.), WALSH (T. F.), ZERWAS (P. M.), Nucl. Phys. B, 1980, 174, 424.
[18] BETHE (H.), HEITLER (W.), Proc. R. Soc. London A, 1934, 146, 83.
[19] WAGNER (W.), Proceedings XX International Conference in High Energy Physics, Madison, Wisconsin, 1980.
[20] WITTEN (E.), Nucl. Phys. B, 1977, 120, 189.
FRAZER (W. R.), GUNION (J. F.), Phys. Rev. D, 1979, 20, 147.
LLEWELLYN SMITH (Ch.), Phys. Lett., 1978, 79B, 83.
[21] BARDEEN (W. A.), BURAS (A. J.), Phys. Rev. D, 1979, 20, 166.
DUKE (D. W.), OWENS (J. F.), Phys. Rev. D, 1980, 22, 2280.
[22] BERGER (Ch.) et al., PLUTO Collaboration, Phys. Lett., 1981, 107B, 168.
[23] FRAZER (W.), Proceedings Fourth International Colloquium on Photon-Photon Interactions, Paris, France, 1981, ed. G. W. Snow.